SPIRE-LAM-PUB-002091

Optical alignment verification of the Herschel - SPIRE Instrument

Kjetil Dohlen*[a], Alain Origne[a], Marc Ferlet[b]
[a]Laboratoire d'Astrophysique de Marseille, OAMP, CNRS, Université de Provence,
2 Place Le Verrier, 13248 Marseille Cedex 4, France
[b]Rutherford Appelton Laboratory, Chilton Didcot, Oxfordshire OX11 0QX, UK

ABSTRACT

The SPectral and Photometric Imaging REceiver (SPIRE) will be launched in 2007 as one of three instruments on ESA's sub-millimetric space telescope Herschel. It covers the 200-670 micron spectral range with a three-band, 4'x8' field-of-view (FOV) photometer and a dual-band, 2.6' diameter FOV imaging Fourier transform spectrometer. Alignment verification of the instrument is accomplished optically by means of OGSE based on classical alignment telescopes and specially designed equipment. The main purpose of this process is to make sure the internal instrument cold stop is aligned with the telescope exit pupil, and that it stays aligned as the instrument is taken down to its 4K operating temperature. Optical alignment verification also includes measurement of pupil imaging quality and characterisation of the instrument wavefront error. For the latter, a Hartmann test is implemented, allowing estimation of the main aberration terms and comparison with the ideal instrument. This paper describes the philosophy of the alignment plan and presents the main results obtained during alignment of the structural and thermal model.

Keywords: Alignment procedures, PSD, sub-millimetric, cryogenic, space instrumentation

1. INTRODUCTION

ESA's Herschel mission[1] consists of a telescope with a 3.5 m diameter primary mirror passively cooled to 80 K, and a cryostat containing the instruments and a reservoir of liquid helium. SPIRE[2], one of the three focal plane instruments, is dedicated to imaging and spectroscopic studies of deep extra-galactic and galactic sources. Based on arrays of bolometer detectors, the instrument covers the 200-670 μm spectral range, of particular importance for determining the history of star formation in galaxies and the early stages of star formation in the interstellar medium. Separated into two parts, the instrument[2] incorporates a three-band photometric camera with a 4′ x 8′ field of view (FOV) designed for deep surveys, and a dual-channel imaging Fourier transform spectrometer (FTS)[4] with a 2.6' diameter circular FOV and a nominal resolving power variable from 20 through to 1000.

The 3.5m Herschel telescope (Figure 1 a) is a Cassegrain system and provides a well-corrected but highly curved image at a focal ratio of f/8.68. SPIRE uses an off-axis part of the telescope FOV and its object surface is therefore tilted with respect to the central (gut) ray. In the common path of the SPIRE instrument (Figure 1 b), CM3, an off-axis ellipsoid, projects an image of the telescope pupil, materialized at the secondary mirror (M2), onto CM4. This is a flat mirror whose orientation is adjustable in flight to permit ±2′ off-field chopping along one axis and ±30′′ fine beam steering motion for Nyquist sampling along both axes. The toric CM5 mirror re-images the image plane onto PM6 and SM6, pick-off mirrors for the photometer and spectrometer, respectively. PM6 sends the beam into an Offner-type relay system consisting of three spherical mirrors, PM7 (concave), PM8 (convex), and PM9 (concave), providing an easily accessible pupil image between PM8 and PM9 in which the cold stop (PCS) is located, and sufficient back-focal length to fit two dichroic beam dividers (PDIC1 and 2), fold mirrors, and bolometer array modules. The cold stop materializes the separation between the 4K cavity surrounding the entire instrument and the 2K cavity to which the array modules are bolted. The bolometers themselves are maintained at 300mK by a He3 cryo cooler.

Figure 1 (c) shows a ray diagram of the spectrometer. SM6 directs the beam through a hole in the optical bench and the flat SM7 redirects it into a plane separated by 170 mm from the photometer plane. A toric relay mirror (SM8A) focuses

* kjetil.dohlen@oamp.fr; phone +33 4 95 09 41 24; fax +33 4 91 62 11 90; http://www.oamp.fr/

the beam to an intermediate image plane located just after the first beam splitter (SBS1). Each interferometer arm (A and B) has individual, spherical collimator and camera mirrors (SM9 and 10, respectively). The collimated beams are redirected by a couple of back-to-back roof-top mirrors (RTA and RTB) mounted on a cryogenic linear translation mechanism[4]. A pair of toric relay mirrors (SM11A and B) focuses the beams onto the bolometer arrays via fold mirrors (SM12A and B). The spectrometer cold stop (SCS) is placed in a pupil image located between SM6 and SM7.

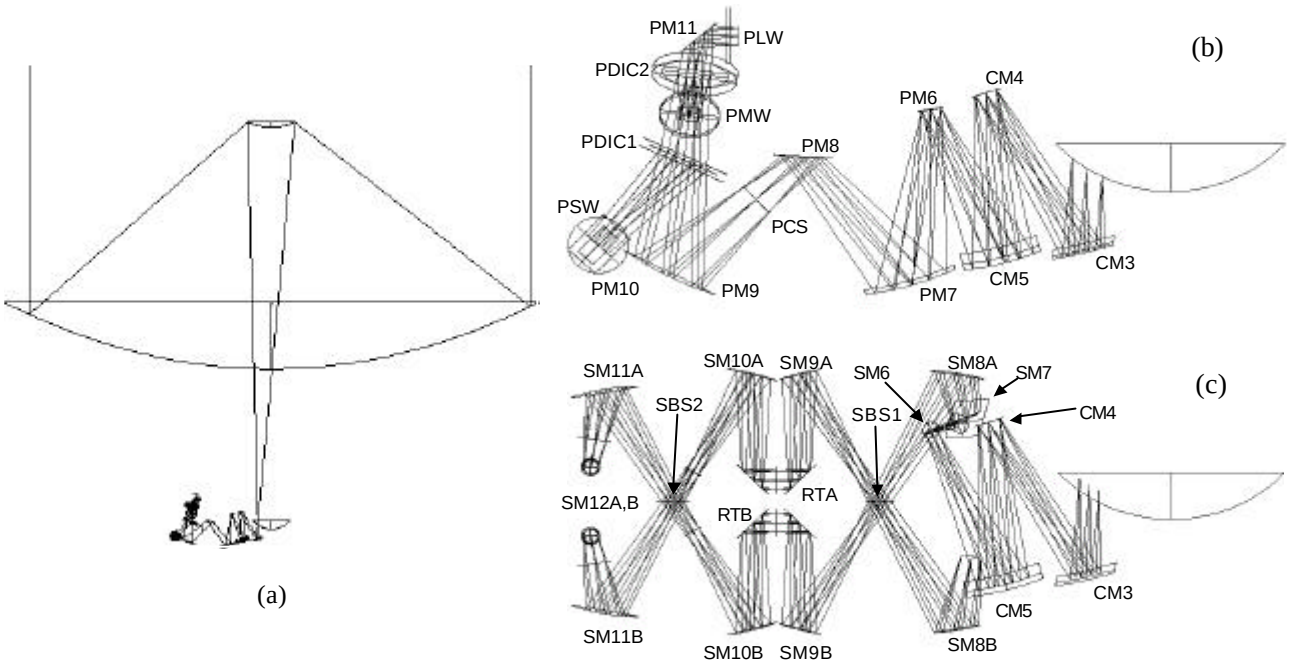

Figure 1. Ray diagram of the FIRST telescope with the SPIRE instrument to the same scale (a). The primary mirror has a diameter of 3.5 m and the SPIRE instrument is about 500 mm wide. Ray diagrams of the SPIRE photometer (b) and spectrometer (c).

Great importance is attached to the alignment and image quality of the internal instrument cold stops, onto the telescope pupil, located at the telescope secondary mirror (M2). This affects the overall instrument transmission and the amount of background signal collected, hence directly touching the scientific performance of the instrument. It is the role of the instrument alignment verification to ensure that the alignment budget is met, and to indicate, if necessary, the remedial actions to be taken.

Alignment of the SPIRE instrument is performed according to a philosophy based on high-precision machining and pre-assembly 3D measurements, and a program of optical alignment checks during and after assembly. Nominally, no adjustments should be necessary, but if a serious misalignment is detected, its compensation will be possible by re-machining of certain mirror stands. Alignment verification of the instrument with respect to the telescope axis and pupil is performed using a standard micro alignment telescope (MAT), theodolites, and an optical bench simulator containing a set of reference mirrors accurately located with respect to the instrument interface points. Verification of image quality and internal alignment stability is effectuated using a set of alignment tools (sources, reticules, …) mounted in strategic positions in the optical train (cold stops and image planes).

The instrument error budget[5] allocates an alignment tolerance of 0.1mm and 1′ to each mirror in the instrument, producing an expected relative pupil displacement ($\Delta R/R$, where ΔR is pupil displacement and R is pupil radius) due to internal misalignments of 4.0%. On top of this there is an allocation of 2.6% for external alignment errors, i.e. the mounting of SPIRE onto the telescope optical bench, the expected telescope alignment error[6] of 6.1%, and the theoretical design residual (pupil aberrations) of 5.0%. The total instrument budget, estimated by square summing of the

alignment errors and summing of the design residual, is 12.7%, which corresponds to an 8% reduction in instrumental transmission.

In this paper we describe the main points in the alignment plan and present results obtained from the ambient and cryogenic alignment verifications of the structural and thermal model (STM) effectuated during the summer of 2003. But before showing these results, we discuss the mirror surface requirements imposed by alignment in the visible.

2. SURFACE QUALITY REQUIREMENTS

While the scientific wavelength range of the instrument requires surface roughness in the micron range, alignment verification at visible wavelengths imposes far more stringent specifications. A roughness specification per surface of 10nm rms was set, representing a quality commonly attained for diamond turned aluminium mirrors and assumed to be more than good enough for our purposes. In particular, this quality has been obtained for the mirrors in the ISO-LWS instrument for which a similar alignment strategy was implemented some 10 years ago. Various technical problems during machining of the mirrors prevented the achievement of this quality, and we were led to analyse more deeply the real requirements in order to decide whether or not to accept the mirrors.

The alignment verification consists of projecting the shadow of alignment tools placed in the instrument pupils, backlit by point sources placed in the instrument focal plane, through the system and detected in the telescope pupil plane. In most cases, the tools contain a pattern of narrow slits, a few 1/10 mm wide and a few mm long. In order to observe these projections, the transmission through the instrument must provide sufficient contrast between the peak intensity within the slit and the intensity outside of the slit. A contrast ratio of at least 10 would be preferable, but 3 is acceptable. We propose that this requirement may be formulated in terms of the one-dimensional power spectral density (PSD_{1D}) of the transmitted wavefront.

The power spectral density (PSD) of a function equals the square modulus of its Fourier transform. For a two-dimensional optical surface, the PSD is naturally two-dimensional, and describes the spectral distribution of the surface irregularities present. Effectively, the surface may be considered as a sum of sinusoidal phase gratings of different frequencies and orientations, each grating corresponding to a point in the PSD plane. By diffraction theory, each grating deflects a part of the light into a certain direction depending upon the grating frequency, and so the surface PSD is closely related to the optical point spread function (PSF) produced by the surface.

Another function commonly used to characterize surface irregularities is the one-dimensional PSD (PSD_{1D}), obtained by integrating the surface PSD along one axis. Since the optical line spread function (LSF) is obtained from the PSF by the same mathematical process, it is clear that the PSD_{1D} is related to the LSF of a surface.

As detailed by Elson and Benett[7], the PSD_{1D} of a surface can be estimated by calculating the averaged PSD from a large number of 1D surface profiles. In practice, this is typically achieved by dividing a long surface trace into a number of short segments. The length of each segment must be compatible with the spatial frequency resolution required, and the sample separation must be compatible with the required bandwith of the PSD.

At a distance sufficiently far from the specular image, the surface scatter effects dominate over pupil diffraction effects, and the LSF is related to the PSD_{1D} for a reflecting surface by the approximation

$$LSF(b) \approx (4p/l)^2 PSD_{1D}(f), \quad (1)$$

where b is angular distance from the source, f is spatial frequency, and l is wavelength. Note that the factor 4 includes the factor 2 introduced by reflection. By Fourier optics theory, the intensity profile of a slit image equals the geometrical slit image convolved with the LSF, and so, sufficiently far from the slit centre:

$$I(b) = S(b) \otimes LSF(b) = S(b) \otimes PSD_{1D}(f), \quad (2)$$

The grating equation relates angular separation to spatial frequency by the small-angle approximatio $\beta = f\lambda$. For a slit of angular width $\Delta\beta$ as seen from the surface, the corresponding spatial frequency range is therefore $\Delta f = \Delta\beta/\lambda$. As long as the PSD_{1D} is slowly varying over the range Δf, the intensity at a distance β from the slit centre may then be estimated from the PSD_{1D} at the corresponding frequency f by

$$I(\beta) \approx (4\pi/\lambda)^2 \, PSD_{1D}(f) \, \Delta\beta/\lambda \, . \tag{3}$$

If the PSD_{1D} is given in terms of nm^2/mm^{-1} , then it is convenient to express wavelengths in nm and angular width in μ-radians.

For a system composed of N optical surfaces, each having a different PSD, each surface adds to the total wavefront at a different spatial scale, h_i. We then have, for the i^{th} surface, $f_i = h_i\beta/\lambda$, and $\Delta f_i = h_i\Delta\beta/\lambda$. Although wavefronts add coherently, if we consider surface defects to be random and independent, then simple addition of PSDs gives a good representation of the total PSD. Eq (3) may therefore be generalized for an N-surface system as:

$$I(\beta) \approx (4\pi/\lambda)^2 \, \Delta\beta/\lambda \sum_i h_i PSD_{1D\,i}(h_i\beta/\lambda) \, . \tag{4}$$

In the case of the photometer, N = 5 mirrors (CM3, CM5, CM6, CM7, CM8; CM4 is excluded since it is in a pupil-conjugate plane) are involved in the imagery between the photometer cold stop (PCS) and the telescope pupil plane in which measurements are made. The apparent angular width of the 0.3mm wide slit in the CS plane varies between 0.6 mrad and 1.5 mrad, with a mean of 1.1 mrad, corresponding to 2.8mm in the M2 plane. Assuming the PSD to be the same for all the mirrors, and using the mean angular slit width, eq. (4) degenerates into:

$$I(\beta) \approx N(4\pi/\lambda)^2 \, PSD_{1D\,i}(f) \, \Delta\beta/\lambda \, . \tag{5}$$

This simplified expression allows us to give a surface specification in terms of PSD_{1D}. For a contrast better than 3 (goal 10), we require $I(\beta>\Delta\beta) < 0.33$ (goal 0.1). For $\Delta\beta$ = 1.1mrad, corresponding to f = 1.8mm^{-1} at λ = 600nm, and with N = 5, this translates into:

$$PSD_{1D\,i} < 75 \; nm^2/mm^{-1} \text{ (goal 25 } nm^2/mm^{-1}) \text{ for } f > 1.8 \; mm^{-1}. \tag{6}$$

To illustrate the use of this criterion, Figure 2 shows form-suppressed profiles of two different mirrors, a typical STM mirror (structural and thermal model, upper trace) and one from the first lot of PFM mirrors (proto-flight model, lower trace). Figure 3 shows PSD_{1D} for each profile calculated according Elson and Benett[7] using ten 2mm long profile segments. While the STM mirrors were judged acceptable, with a PSD below spec over the entire range, the first lot of PFM mirrors, whose PSD is below the goal in the high frequencies but stays above the specified limit well beyond the required frequency limit, was rejected. This decision was comforted by the calculation of a simulated LSF, see Figure 4. Clearly, while the STM mirror has a width compatible with imaging of milli-radian sized objects, the first-lot PFM mirror does not get anywhere near the required performance. According to the mirror manufacturer, the observed improvement in the high-frequency range was probably due to the use of a higher quality diamond tool, while the reduced low-frequency performance was due to a defective position sensor.

Following this analysis and servicing of the diamond turning lathe, the defective mirrors were re-machined to excellent standard, see Figure 3 (black dotted line).

A validation of the specification criterion was obtained during the STM alignment campaign in May 2003. Figure 5 (left panel) shows an image of a 0.3mm wide slit situated in the photometer cold-stop as projected onto the telescope pupil plane. The right panel shows the profile along the line indicated in the picture. The FWHM of the projected slit image is 2.2mm, which corresponds well with the expected value. The peak-to-foot contrast ratio, taking into account a zero-offset of about 9 units, is 108/26 = 4.2. Better than spec (3) and not quite up to the goal (10), this performance is in good agreement with the performance predicted from the measured PSD_{1D}.

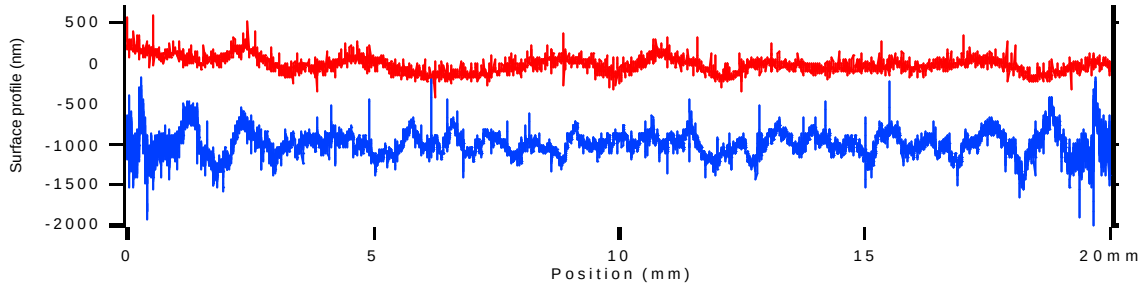

Figure 2. Form-suppressed profiles of the STM mirror (upper trace, red) and one of the PFM mirrors (lower trace, blue).

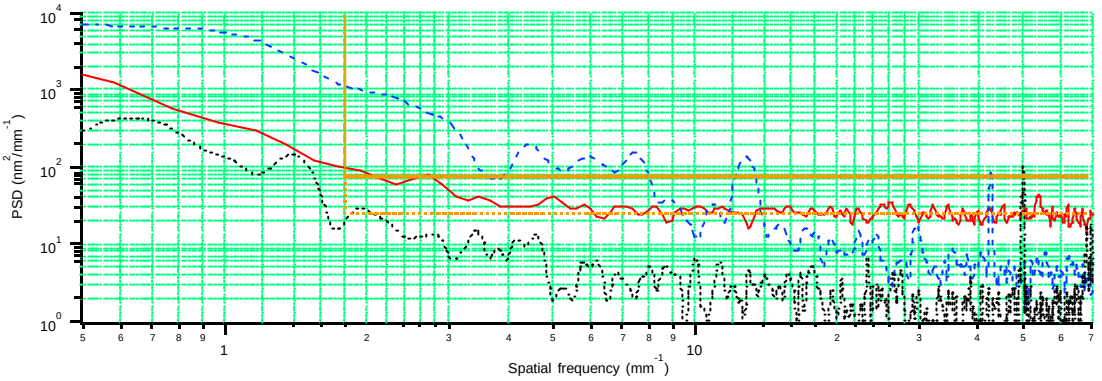

Figure 3. Typical average PSD obtained from measurements of SPIRE mirrors. STM (full line, red), first PFM lot (broken line, blue), and second PFM lot (dotted line, black).

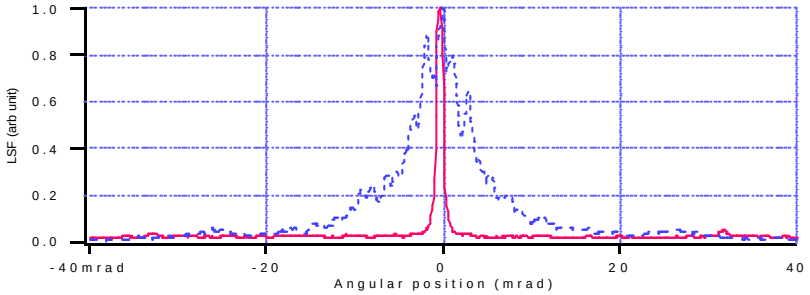

Figure 4. Simulated LSF for an STM mirror (full line, red) and for a first-lot PFM mirror (broken line, blue).

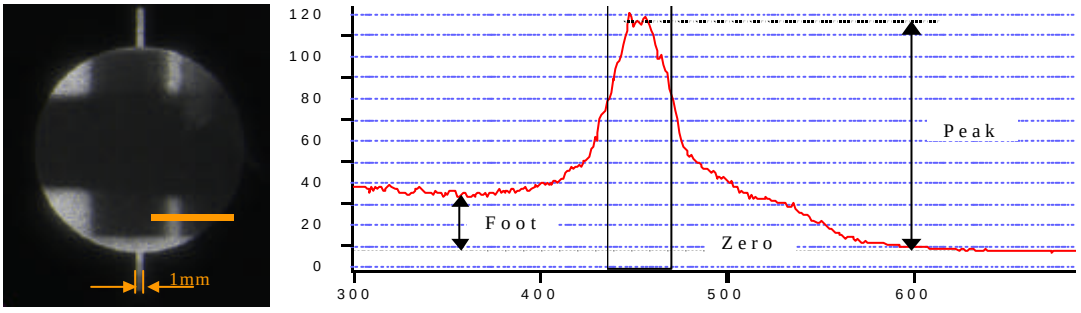

Figure 5. Image of PCS tool slits taken through a M2 tool hole (left) and intensity profile (right).

3. EXTERNAL PUPIL ALIGNMENT

The SPIRE mirrors are mounted in the structure via a standard interface. For each mirror, this consists of a 20mm diameter flat surface and a 8.5mm diameter, 20mm long central spigot that ends in an M8 screw. The spigot axis is supposed to be coincident with the local surface normal, but dimensional measurements of the STM mirrors showed that some of them suffer from several minutes of misalignment. In particular, this was the case for the CM3 mirror, an off-axis aspheric mirror, which suffered from 27' misalignment due to an error in the manufacturing setup. The sources of these misalignments have been determined and corrected for in the PFM mirrors.

During the May 2003 alignment campaign, the STM pupil alignment was measured and compared with simulations of the as-built system. Figure 6 (a) shows the photometer side of the instrument during these tests. A strong, fibre-fed light source placed in the instrument focus projected a shadow of the cold stop mask onto the telescope M2 plane; see Figure 6 (b). The recorded deviation of the actual instrument gut ray impact from the centre of the telescope pupil was 46.8mm along the SPIRE Z axis and -4.0mm along the SPIRE Y axis. This is within 1.7mm of the deviation obtained from as-built simulations taking into account measured spigot misalignments, indicating deviations of 45.3mm and 3.1mm, respectively. The residual error, representative of other error sources such as the structure manufacture and the alignment setup, represents a relative pupil alignment error of 1.1%, well within the SPIRE error budget allocation of 4.0% (6.2mm) for internal instrument alignment and 2.6% (4.0mm) for external instrument alignment.

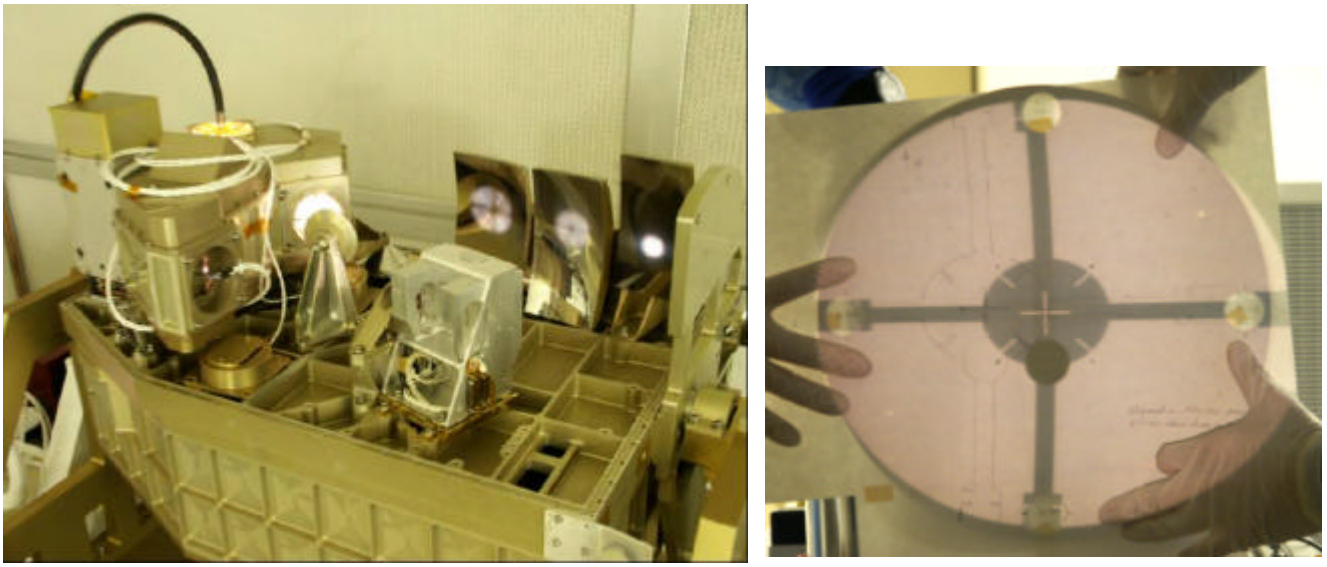

(a) (b)

Figure 6. View of the photometer side of the instrument during cold-stop alignment verification (a). Notice the bright spots seen on all the mirrors representing the projection of the cold-stop (PCS) tool.
Shadow of the PCS tool projected onto the M2 tool (b). For clarity, a sheet of paper is held in front of the M2 tool. The shadow seen here is obtained after lateral adjustment of the M2 tool so that its centre coincides with the central cross of the PCS tool. The pencil trace on the paper shows the original PCS tool shadow obtained with the M2 tool aligned according to the theoretical telescope axis.

4. PUPIL ABERRATIONS

Pupil aberrations are measured by observing the shadow of the slits machined into the cold stop mask at the pupil edge as seen through holes with corresponding slits in the M2 tool. This observation is made possible by the use of a specially designed loupe interfaced with a CCD camera, see Figure 7 and a tool located in the instrument focal plane containing five LED light sources, one in each corner (A, B, C, D) and one in the centre (E). Unfortunately, one LED

(D) was faulty. Figure 8 shows images taken with the four working LEDs, the image corresponding to field point E indicates the orientation of the images and illustrates the method used for analysis of the images:

- Image scale (mm/pixel) is determined by considering the M2-tool hole diameter.
- Position of the M2-tool is given by point P
- Position of the CS-tool shadow is given by point Q
- Pupil aberrations are the variations in the difference between the coordinates of P and Q.

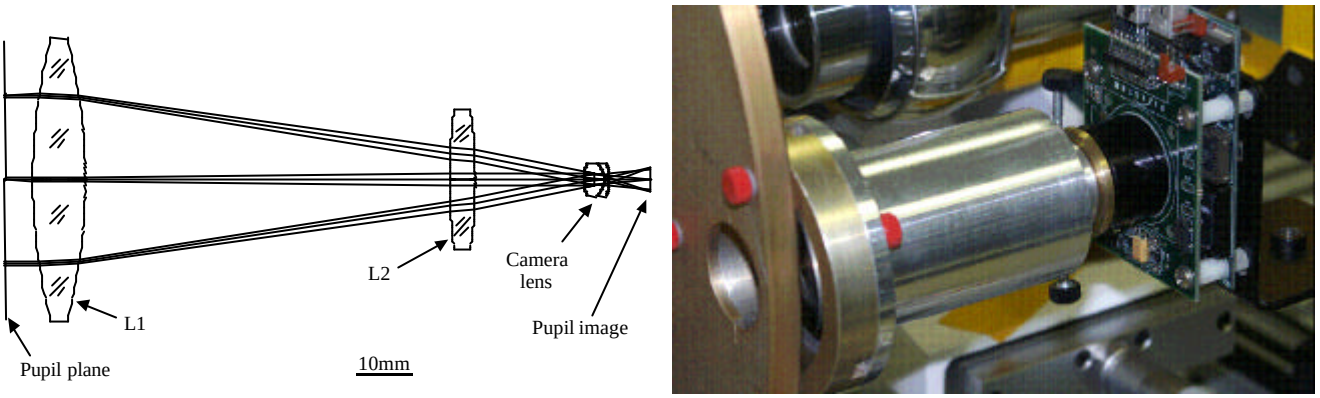

Figure 7. Optical design (a) and practical realization (b) of the pupil loupe used for measurement of pupil aberrations. The photo shows the loupe mounted onto the M2-tool and with the CCD camera attached.

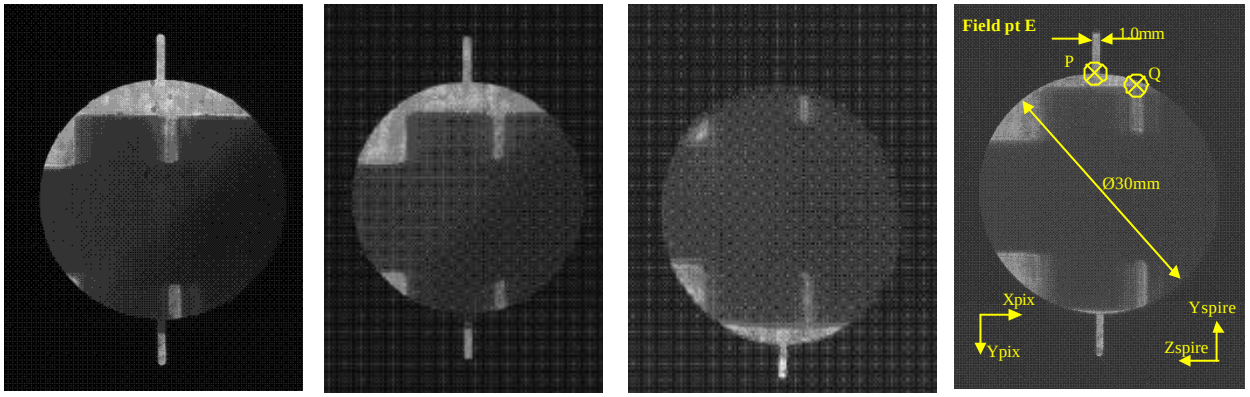

Figure 8. Images observed with the Loupe through the Right-hand M2-tool hole for D-tool sources A, B, C, and E.

While it was foreseen to measure pupil aberrations in four positions around the pupil rim ("Up", "Down", "Left" and "Right", with reference to the view of Figure 6 b), time constraints only allowed us to perform these measurements for one position ("Right") during the STM campaign. Figure 9 shows expected pupil aberrations at each of the four positions, and the measured results are added in the panel corresponding to the "Right" position. The average difference between predicted and measured aberrations is 1mm, indicating that the pupil aberrations of the as-built STM are in good agreement with the designed system.

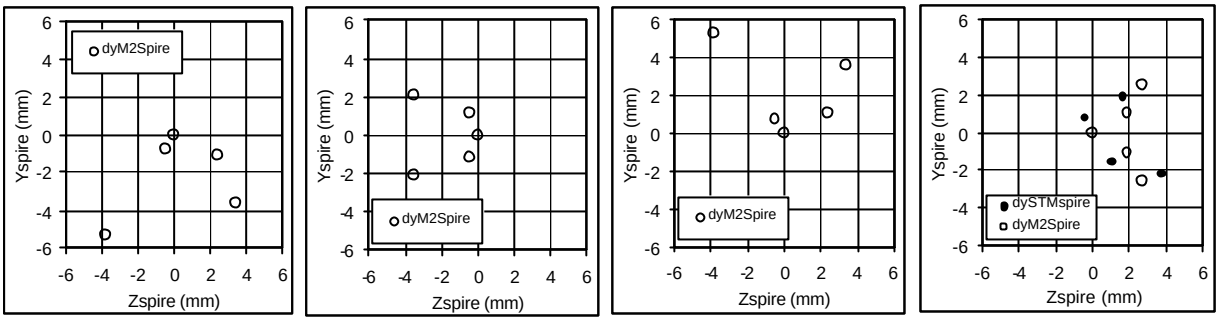

Up Left Down Right

Figure 9. Pupil spot diagrams for each of the four positions around the pupil edge. The spots represent M2 impact points for rays emanating from each focal plane LED and passing through each of four points around the cold stop edge. Open circles correspond to theoretical values; filled circles are measurement results ("Right" only).

5. IMAGE QUALITY

Measurement of SPIRE image quality was done using a Hartmann test. A specially designed lunette, containing two lenses and a CCD camera, is placed in front of the instrument entrance, see Figure 10 (a), and provides an image of the instrument focal plane in a telecentric beam. Sliding the CCD camera through this focus provides equally scaled intra and extra focal images. When a Hartmann screen containing 21 holes in a regular grid is placed in the instrument's internal cold stop pupil, the extra and intra focal images show up as distorted images of the screen (see Figure 10 b). Determining the positions of Hartmann holes in each image allows calculation of the wavefront slopes, hence quantitative determination of image quality in terms of Zernike polynomials.

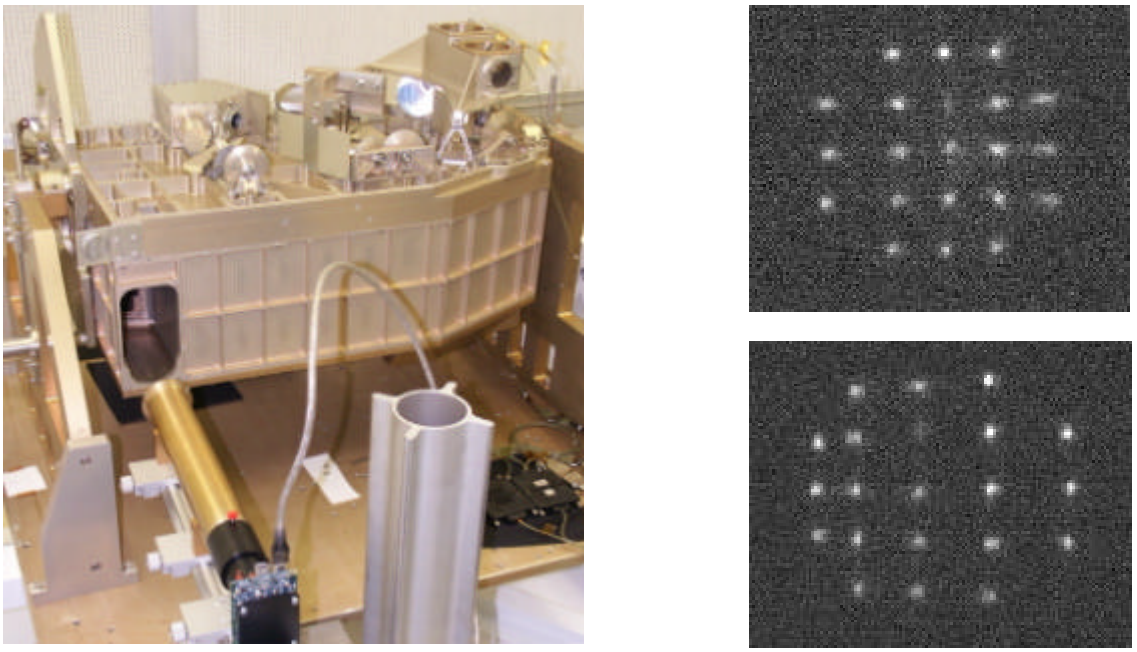

(a) (b)

Figure 10. View of the spectrometer side of the instrument during the Hartmann test (a) and typical extra and intra-focal images (b).

The Hartmann test provides verifications of image quality and focus position. 14 Zernike coefficients up to fifth-order coma are calculated by least squares fitting of the measured slope data to differentiated versions of the Zernike

polynomials[8]. It was found useful to present the data in two different ways. First, the slope data was used directly to create spot diagrams, which were compared with raytracing spot diagrams and provided qualitative verification of the measured results, see Figure 11. Second, comparison of the fitted Zernike coefficients with theoretically obtained coefficients provided a powerful tool for quantitative analysis of the as-built system. Table 1 shows a condensed version of this list, where the two coefficients of asymmetrical Zernike terms have been root-sum-squared. These coefficients represent the contribution of each aberration to the total rms wavefront error (WFE).

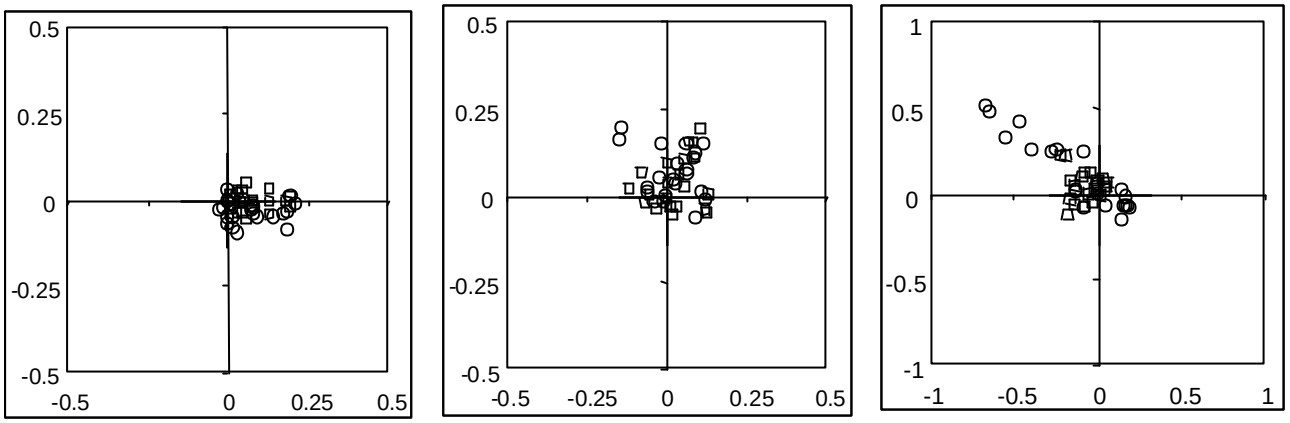

Figure 11. Comparison of spot diagrams generated from the measured slopes (circles) with theoretical diagrams generated by raytracing (squares) for Photometer field points E (a) and B (b), and the Spectrometer (c). Units along the axes are mm in the final f/5 SPIRE focii.

Table 1. Comparison of Zernike coefficients given by raytracing and measured. The coefficients represent rms contribution in μm. Also listed are total rms WFE and Strehl ratio at 250μm.

	Photometer				Spectrometer	
	Field pt E		Field pt B			
Aberration	**Raytracing**	**Measured**	**Raytracing**	**Measured**	**Raytracing**	**Measured**
Focus (Z3)	0.18	1.45	0.44	0.20	2.64	4.47
Astigmatism	0.72	1.03	2.74	2.35	1.44	6.42
Coma	0.87	0.94	0.63	0.71	0.35	1.90
SphAb	0.11	0.29	0.11	0.52	0.02	0.45
Tri5	0.33	0.49	0.21	0.36	0.63	0.65
Ast5	0.05	0.24	0.04	0.08	0.09	0.16
Coma5	0.01	0.08	0.01	0.09	0.00	0.40
WFE RMS	**1.20**	**2.10**	**2.85**	**2.54**	**3.09**	**8.10**
Strehl 250um	**0.999**	**0.997**	**0.995**	**0.996**	**0.994**	**0.959**

Quantitative focus determination was an important product of this analysis. The front-focal distance of the lunette was precisely calibrated, and the focus error (Δ) was determined from the Zernike focus coefficient (Z3) according to:

$$\Delta = 16\sqrt{3}\, F^2\, Z3 = k\, Z3,$$

where F is the focal ratio and k is a numerical factor depending upon the focal ratio. In the telescope focus, where F = 8.68, we have k = 2088, and in the instrument focii, where F = 5, we have k = 690. For the photometer, the focus error (difference between raytracing and measured) represents a WFE of 1.3μm rms at the central field point. Although this corresponds to a defocus at the detector of 0.9mm (i.e. 2.7mm at the telescope focus), it is of no consequence for the instrument error budget. The spectrometer is slightly more defocalized, with a WFE contribution of 1.8μm,

corresponding to a defocus of 1.3mm at the detector, which is still acceptable. These focus errors correspond well with the cumulative effect of mirror curvature errors, specified to $\Delta R/R < 10^{-3}$.

Comparison of the other wavefront terms confirms that the photometer is in excellent agreement with the designed system. Still, a certain difference is noticed in the astigmatism term, which corresponds to astigmatic deformations detected during interferometric characterization on some of the mirror surfaces, see Figure 12 (a), possibly due to stress release. Although the surface deformations of these mirrors are within specifications, its presence indicates an insufficient thermal cycling procedure for the mirror substrates. A slight increase in spherical aberration is also detected; this corresponds to the presence in some of the mirrors of axi-symmetrical deformations, see Figure 12 (c).

(a) SM7_02
Mainly astigmatism

(b) SM12a_01
Mainly coma

(c) SM9a_01
Mainly spherical aberration

Figure 12. Interferometric fringes measured for three of the SPIRE mirrors representative of three types of deformations.

In the spectrometer, the astigmatism discrepancy is much larger (~5µm, see Table 1), but its source is well identified. During the Hartmann test, it became immediately evident that the as-built STM model suffered from an astigmatism corresponding to a 18mm longitudinal separation between tangential and sagittal foci. This represents a WFE of 20µm rms, twice the total instrument error budget. Its cause was quickly identified to an erroneously positioned doweling pin for the toroidal mirror SM8A, causing an azimuthal rotation of this mirror through 12.44º. Removing the dowel allowed rotating the mirror such as to minimize visually the residual aberration observed with the Hartmann lunette (Figure 13). By this method, the SM8A rotation was adjusted to within some 3º of the optimal, hence the residual astigmatism error reported in Table 1. Appropriate action has been taken to avoid this error in the PFM structure. Much smaller but still significant differences are also seen in the coma and spherical aberration values, probably due to deformed mirror surfaces, see Figure 12 (b) and (c), as discussed above.

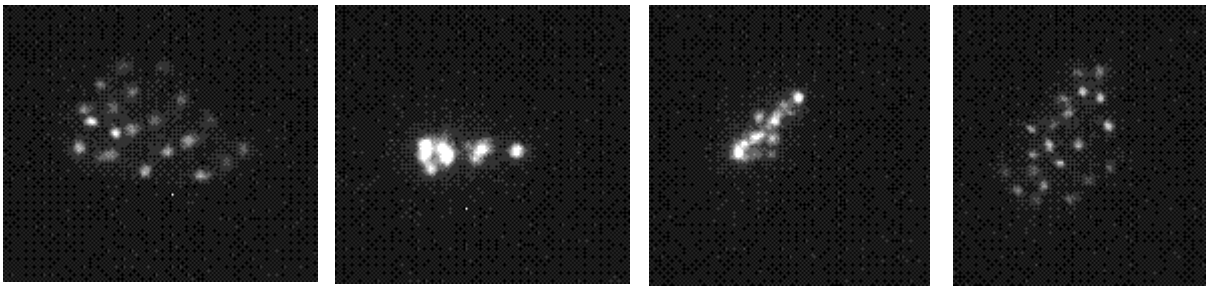

a: ~9º b: ~12º c: ~15º d: ~18º

Figure 13. Images taken at approximately 3º intervals near the optimal rotation of SM8A.

6. CRYOGENIC ALIGNMENT VERIFICATIONS

A procedure for alignment verification during passage through thermal vacuum has been devised in order to validate the internal and external stability of the instrument. This procedure primarily verifies that the projection of the instrument pupil onto the telescope pupil remains stable as a function of temperature between 300K and 10K. Also, relative angular movements between the SPIRE optical bench (SOB) and the Herschel optical bench simulator (HOB) are monitored as an aid to tracking any anomalous behaviour in the pupil alignment.

As for the external pupil alignment verification at ambient, cryogenic pupil alignment is verified by observing the cold stop tools, back-lit by cryo-compatible near IR LEDs[9] located in the instrument focal planes and projected onto the telescope pupil plane. The telescope pupil is located by the aid of a reference cube mounted on the HOB, whose top face is perpendicular to the telescope axis and equipped with a cross hair materializing the position of the axis. The MAT, placed just behind the telescope pupil plane, is aligned with the HOB cube. Since the HOB with the instrument mounted on it is free to move slightly within the cryostat, the MAT alignment is repeated every time a measurement is effectuated. A pupil simulator consisting of a plexiglas screen (M2 screen) is located in the telescope pupil plane.

Measurement of relative movement between the SOB and the HOB is done by the aid of two reference cubes, one on the HOB and one on the SOB. Theodolites are used to determine the orientation of each cube, using the optical cryostat window as a reference. Uncoated and sufficiently wedged to separate the reflection from each face, auto collimation on the window is easily obtained. Although a certain flexure of the window is expected in going from ambient pressure to vacuum, no significant variations with temperature are expected.

A measurement sequence consists of (1) aligning the MAT with the telescope axis, (2) aligning the M2 screen with the MAT axis, (3) lighting up the LED in the centre of the photometer image plane and observing the projection of the photometer cold stop on the M2 screen by the aid of the M2 loupe (Figure 7), (4) repeating pt. (3) for the LED in the centre of the spectrometer image plane, and (5) measuring the relative position of the SOB and HOB cubes.

Cryogenic alignment verifications were done during a five-week cryo-campaign effectuated in the summer of 2003. Five alignment measurements were made; at ambient, warm vacuum, 100K vacuum, 10K vacuum, and back at warm vacuum. Figure 14 (a) shows the resulting relative position errors of the photometer (blue squares) and spectrometer (yellow circles) pupils, as well as the angular deviations between the SOB and HOB cubes, translated into corresponding pupil movements (red triangles). Each set of measurements has been centred to put its centre of gravity at the origin of the plot. Clearly, the pupil measurement data shows a larger dispersion than the theodolite measurements. In Figure 14 (b), the amplitude of the relative pupil position error is plotted against temperature. No clear temperature effect can be discerned. The precision of the theodolite measurements is estimated to 0.1mm, and the observed variations of ±0.3mm must therefore be considered representative of real differences in orientation between the HOB and the SOB, perhaps due to thermal gradients. However, the ±1mm dispersion in pupil position measurements corresponds with the estimated precision in the determination of the centre of the projected cross hairs. In any case, the registered pupil movements are well within the tolerable amounts.

7. CONCLUSIONS

We have described the ambient and cryogenic alignment verification procedures for the SPIRE instrument and the results of its practical execution during the STM campaigns. The use of visible light for these tests sets relatively strict requirements for mirror surface quality, and a formalism elaborated in Sec. 2 of this paper allows specification and critical acceptance analysis of each mirror in terms of the 1D surface PSD.

Contrary to what is commonly found in optical instruments, the most critical performance criterion for the sub-millimetric SPIRE instrument is pupil alignment and pupil aberrations rather than image quality. Verification of pupil alignment is done by projecting the internal instrument pupil onto the theoretical telescope pupil plane, materialized by the aid of an alignment telescope and reference mirrors mounted on the instrument. Although some of the STM mirrors suffered from severe angular misalignments, the comparison between measurements and as-built simulations was good, confirming that both the mechanical structure and the alignment procedure have the appropriate accuracy.

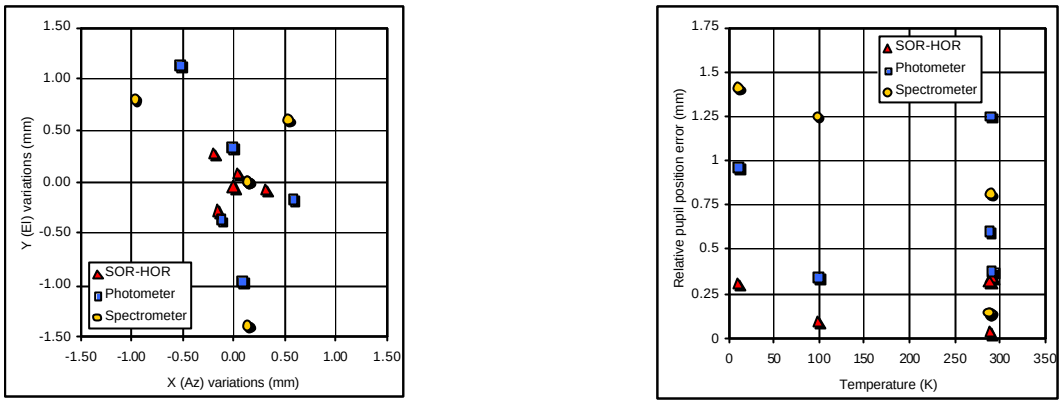

(a) (b)

Figure 14. (a): Relative position of the photometer pupil (blue squares) and spectrometer pupil (yellow circles), as well as the angular deviation between the SOB and HOB cubes, translated into corresponding pupil movements (red triangles), for each of the five alignment measurements effectuated during the summer 2003 cryo campaign. Each set of measurements has been centred to put its centre of gravity at the origin of the plot.
(b): Amplitude of the relative pupil position errors plotted against temperature.

It appears that the main cause for image quality deterioration is low-order surface deformations observed in some flat or spherical mirrors. Although well within the error budget allocations, the presence of such deformations indicates the occurrence of stress release after machining of the mirror surfaces, possibly due to insufficient thermal cycling of the mirror substrates. A different cause for image deterioration, due to a faulty doweling pin location, was also detected. It is possible that this error, causing a 20µm rms WFE, would have passed undetected if the Hartmann test for image quality characterization had not been implemented. Such an error, which would have brought the Strehl ratio at 250µm to below 60% instead of the required 90%, would have had a non-negligible impact upon the SPIRE science output.

REFERENCES

1. G.L. Pilbratt, "The Herschel mission, scientific objectives,and this meeting," Proc. Symposium *The Promise of the Herschel Space Observatory* 12-15 December 2000, Toledo, Spain, ESA SP-460, eds.G.L.Pilbratt, J. Cernicharo, A.M. Heras, T. Prusti, & R. Harris, pp. 13-20 (2001).
2. M.J.Griffin ,B.M.Swinyard ,and L.Vigroux, "The SPIRE instrument for Herschel," Proc. Symposium *The Promise of the Herschel Space Observatory* 12-15 December 2000, Toledo, Spain, ESA SP-460, eds.G.L.Pilbratt, J. Cernicharo, A.M. Heras, T. Prusti, & R. Harris, pp. 37-44 (2001).
3. K. Dohlen, A. Origné, D. Pouliquen, B. Swinyard, "Optical design of the SPIRE instrument for FIRST", in: *UV, optical, and IR space telescopes and instruments*, J. B. Breckinridge, P. Jacobsen, Eds, Proc. SPIE 4013, pp. 119-128 (2000).
4. B.M. Swinyard, K. Dohlen, D. Ferand, J-P. Baluteau, D. Pouliquen, P. Dargent, G. Michel, J. Martignac, P.A.R. Ade, P.C. Hargrave, M.J. Griffin, D.E. Jennings, M.E. Caldwell, "The FIRST-SPIRE spectrometer, A novel imaging FTS for the Sub-Millimetre", in: *UV, optical, and IR space telescopes and instruments*, J. B. Breckinridge, P. Jacobsen, Eds, Proc. SPIE 4013, pp. 197-207 (2000).
5. K. Dohlen, Herschel-SPIRE: Optical error budgets, LAM document LOOM.KD.SPIRE.2000.002-4 (2002).
6. FIRST alignment plan, ESA document PT-PL-02220 (1996).
7. J. M. Elson, J. M. Bennett, "Calculation of the power spectral density from surface profile data," Appl. Opt. **34**, 201-208 (1995).
8. R. Cublaichini, "Modal wave-front estimation from phase derivative measurements," J. Opt. Soc. Am **69**, pp. 972-977 (1979)
9. G.Michel, K. Dohlen, J. Martignac, J-C. Lecullier, P. Levacher, C. Colin, "An interferential scanning grating position sensor operating in space at 4K", Appl. Opt. **42**, 6305-6313 (2003).